


Article

# The Effect of N, C, Cr, and Nb Content on Silicon Nitride Coatings for Joint Applications

Luimar Correa Filho <sup>1</sup>, Susann Schmidt <sup>2</sup>, Cecilia Goyenola <sup>3</sup>, Charlotte Skjöldebrand <sup>1</sup>,  
Håkan Engqvist <sup>1</sup>, Hans Högberg <sup>3</sup>, Markus Tobler <sup>2</sup> and Cecilia Persson <sup>1,\*</sup>

<sup>1</sup> Division of Applied Materials Science, Department of Materials Science and Engineering, Uppsala University, 751 21 Uppsala, Sweden; luimar.filho@angstrom.uu.se (L.C.F.); charlotte.skjoldebrand@angstrom.uu.se (C.S.); hakan.engqvist@angstrom.uu.se (H.E.)

<sup>2</sup> Ionbond AG, Industriestrasse 9, Dulliken 4657, Switzerland; susann\_Schmidt@gmx.de (S.S.); markus.tobler@ionbond.com (M.T.)

<sup>3</sup> Thin Film Physics Division, Department of Physics, Chemistry and Biology (IFM), Linköping University, 58183 Linköping, Sweden; cecigoyenola@hotmail.com (C.G.); hans.hogberg@liu.se (H.H.)

\* Correspondence: cecilia.persson@angstrom.uu.se; Tel.: +46-0702-489-624

Received: 29 February 2020; Accepted: 14 April 2020; Published: 17 April 2020



**Abstract:** Ceramic coatings deposited on orthopedic implants are an alternative to achieve and maintain high wear resistance of the metallic device, and simultaneously allow for a reduction in metal ion release. Silicon nitride based ( $\text{SiN}_x$ ) coatings deposited by high power impulse magnetron sputtering (HiPIMS) have shown potential for use in joint replacements, as a result of an improved chemical stability in combination with a good adhesion. This study investigated the effect of N, C, Cr, and Nb content on the tribocorrosive performance of 3.7 to 8.8  $\mu\text{m}$  thick  $\text{SiN}_x$  coatings deposited by HiPIMS onto CoCrMo discs. The coating composition was assessed from X-ray photoelectron spectroscopy and the surface roughness by vertical scanning interferometry. Hardness and Young's modulus were measured by nanoindentation and coating adhesion was investigated by scratch tests. Multidirectional wear tests against ultrahigh molecular weight polyethylene pins were performed for 2 million cycles in bovine serum solution (25%) at 37 °C, at an estimated contact pressure of 2.1 MPa. Coatings with a relatively low hardness tended to fail earlier in the wear test, due to chemical reactions and eventually dissolution, accelerated by the tribological contact. In fact, while no definite correlation could be observed between coating composition (N: 42.6–55.5 at %, C: 0–25.7 at %, Cr: 0 or 12.8 at %, and Nb: 0–24.5 at %) and wear performance, it was apparent that high-purity and/or -density coatings (i.e., low oxygen content and high nitrogen content) were desirable to prevent coating and/or counter surface wear or failure. Coatings deposited with a higher energy fulfilled the target profile in terms of low surface roughness ( $R_a < 20 \text{ nm}$ ), adequate adhesion ( $L_{c2} > 30 \text{ N}$ ), chemical stability over time in the tribocorrosive environment, as well as low polymer wear, presenting potential for a future application in joint bearings.

**Keywords:** silicon nitride; coating; joint replacement; wear; adhesion

## 1. Introduction

Total joint replacements (TJR) are surgical procedures carried out most frequently on patients suffering from arthritic pain or bone fractures [1–5]. These procedures are largely considered successful, with success rates up to 90% at 10 years follow-up for total hip replacements (THR) and total knee replacements (TKR) [6,7]. However, the aging and more active population places higher demands on these implants.

Typically, for THRs the femoral head is replaced by a metal alloy (CoCrMo) or ceramic (zirconia-toughened alumina (ZTA)), and the acetabulum by a ceramic or polymer (ultrahigh molecular weight polyethylene (UHMWPE) or cross-linked polyethylene (XLPE)) [8–12]. TKRs are composed of a metallic femoral component (CoCrMo) as well as a polyethylene XLPE insert attached in the tray [3,13–16]. Ceramic coatings on metallic substrates can be used to reduce wear of structural materials, including manufacturing tools as well as joint implants [17,18]. Different types of ceramic coatings are under investigation for hip joint applications (e.g., TiN, DLC, ZrO<sub>2</sub>, ZrN, CrN, and Si<sub>3</sub>N<sub>4</sub>), while TiN and ZrN coatings are already in clinical use in knee implants [19–23]. These transition metal nitride coatings have the expressed purpose of extending the implant's life time, by either preventing or minimizing the body's immune reaction, which might result in osteolysis, aseptic loosening, and ultimately implant revision [24–35].

According to our previous work, SiN<sub>x</sub> based coatings have shown potential as an alternative for joint bearings due to their biocompatibility, high wear resistance and hardness, and reduced metal ion release [36–39]. However, it is challenging to achieve an optimal combination of adhesion, coating density, and reactivity in SiN<sub>x</sub> coatings; a high coating density resulting in a lower reactivity may give an insufficient adhesion to the substrate due to high residual stresses [40]. Alloying with a third element may be an option to improve the chemical stability while maintaining a balance in coating density and adhesion. For silicon nitride, previous studies have shown that the addition of Cr increases oxidation resistance and mechanical properties [41,42], while Nb improves the wear resistance and increases the hardness [43]. In previous studies, we reported that the addition of C altered the surface reactivity of silicon nitride and influenced the coating density and surface morphology [44,45]. In addition, we have shown that an increased N content results in a higher hardness and density [46–48]. In this study, we investigated the effect of N, C, Cr, and Nb content, as well as ion energy, on the properties of silicon nitride (SiN<sub>x</sub>)-based coatings for joint applications, with a focus on their wear performance in a hard-on-soft contact, since, as mentioned above, the counter surface in a joint implant is usually a polyethylene polymer. The coatings were deposited on top of Cr-based interlayers, and were evaluated in terms of chemical composition, surface roughness, mechanical properties, adhesion, and wear resistance in a hard-on-soft contact.

## 2. Materials and Methods

### 2.1. Coating Deposition

Coating deposition was conducted in an industrial coating system, with a chamber volume of about 1 m<sup>3</sup>, equipped with four magnetrons, of which two were operated in unbalanced magnetron sputtering (UBM) and two in high power impulse magnetron sputtering (HiPIMS) mode. The coatings were deposited using 2-fold substrate rotation. The Si targets were operated at average powers of 5 kW and 8 kW in HiPIMS mode, while the Cr and Nb targets were operated in UBM mode at a sputtering power 1 kW for Cr and sputter powers of 1 kW, 2 kW, or 5 kW for Nb. SiN<sub>x</sub> coatings with thicknesses ranging from 3.7 to 8.8 μm were deposited on mirror polished CoCrMo discs. Ion energies were controlled using three different bias voltages (low, medium, and high) as well as average target power settings. The sputter atmosphere was controlled at a pressure of 600 mPa, with N<sub>2</sub>-to-Ar ratios ranging between 17% and 40% and the remaining percentage to reach 100% was Ar. Detailed information can be found in Table 1.

**Table 1.** Description of the coatings and deposition processes used in this study. A pressure of 600 mPa was used for all deposition runs.

Analysis Aim	Coating Designation	Magnetrons				Bias	Gas	
		Si (HIPIMS) (kW)	Cr/Nb (UBM) (kW)	Si (HIPIMS) (kW)	Cr/Nb (UBM) (kW)		N <sub>2</sub> Content (%)	C <sub>2</sub> H <sub>2</sub> Content (%)
Standard coating	Standard	5.0	-	5.0	-	low	40.0	-
Effect of N content in top layer	N-low	5.0	-	5.0	-	low	17.0	-
	N-medium	5.0	-	5.0	-	low	25.0	-
	N-high	5.0	-	5.0	-	low	40.0	-
Effect of C content	C-low	5.0	-	5.0	-	medium	38.0	2.5
	C-high	5.0	-	5.0	-	medium	36.0	4.0
Effect of Nb content	Nb-low	5.0	1.0	5.0	1.0	low	40.0	-
	Nb-medium	5.0	2.0	5.0	2.0	low	40.0	-
	Nb-high	5.0	5.0	5.0	5.0	low	40.0	-
Effect of Cr content	Cr	5.0	1.0	5.0	1.0	low	40.0	-
Effect of deposition energy	Bias-medium	5.0	-	5.0	-	medium	40.0	-
	Bias-high	5.0	-	5.0	-	high	40.0	-
	Si Power-high	8.0	-	8.0	-	low	40.0	-

## 2.2. Compositional Analysis

The composition of the SiN<sub>x</sub> coatings was investigated by X-ray photoelectron spectroscopy (XPS, Axis UltraDLD, Kratos Analytical, Manchester, UK) using monochromatic Al(K<sub>α</sub>) X-ray radiation ( $h\nu = 1486.6$  eV). The base pressure in the analysis chamber during acquisition was  $< 1 \times 10^{-7}$  Pa. The experimental conditions were such that the full width at half maximum (FWHM) of the Ag3d<sub>5/2</sub> peak from the reference Ag sample was 0.45 eV. For all coatings, XPS survey spectra and core levels were recorded on as-received samples and after sputter cleaning. Sputter cleaning consisted of an initial step of 900 s at an Ar<sup>+</sup> beam energy of 2 keV, followed by a second step for 900 s at an Ar<sup>+</sup> beam energy of 4 keV. During sputter cleaning the Ar<sup>+</sup> beam was rastered over an area of  $3 \times 3$  mm<sup>2</sup> at an incidence angle of 20°. Automatic charge compensation was applied throughout the acquisition, using low energy electrons provided by a flood gun. The composition of the coatings was assessed from XPS high-resolution core level spectra recorded from the Si 2p, Ar 2p, N 1s, C 1s, and O 1s regions after sputter cleaning. Core level spectra were analyzed with CasaXPS (v2.3.15, Casa Software Ltd, Teignmouth, UK). A Shirley-type background was subtracted, and the spectra were calibrated using adventitious surface carbon at 284.8 eV as a charge reference. For quantitative analysis of the metal-containing coatings the core levels of the Cr 2p and Nb 3d were applied for determination. The measurement precision for XPS analysis was  $\pm 5\%$  for compositions below 10 at % and  $\pm 2\text{--}3\%$  for compositions above 10 at % [49].

During wear tests and exposure to fetal bovine serum (FBS) solution a reaction occurred, and a white layer was formed on the surface of some coatings. This layer was examined using monochromatic Al (K<sub>α</sub>) X-ray photoelectron spectroscopy (XPS, Quantera II, Physical Electronics (PHI), Eden Prairie, MN, USA). Measurements were conducted on the surface after 2 min of sputtering Ar<sup>+</sup> ions at 500 V and after an additional 20 min at 1 kV, to investigate the coating surface and further down in the coating, respectively. The sample was mounted on a glass slide in order to float the sample and automatic charge compensation was used throughout the measurement. Core level spectra were analyzed in CasaXPS, a Shirley-type background was subtracted, and the spectra were calibrated using adventitious surface carbon at 284.8 eV as a charge reference.

## 2.3. Surface Roughness

The coating roughness was measured before wear testing using optical profilometry, specifically vertical scanning interferometry (VSI) at 10× and a field of view (FOV) of 1.0. Each measurement corresponded to an area of  $451 \times 594$  μm<sup>2</sup>. Typically, four measurements were performed on each sample to obtain R<sub>a</sub> (arithmetic average).

#### 2.4. Nanoindentation

The hardness and elastic modulus of the coatings were measured in a CSIRO UMIS nanoindenter (Fischer-Cripps Laboratories, New South Wales, Australia) equipped with a three-sided Berkovich tip. All films were tested in the load-controlled mode and for calculations a Poisson's ratio of 0.3 was used. For the tests, at least 30 indents with a load of 20 mN were performed [50].

#### 2.5. Scratch Testing

In order to investigate coating adhesion, a scratch test was performed at different time points [51] using a scratch tester (CSEM-Revetest (CSEM, Neuchatel, Switzerland)) with a Rockwell C tip (apex  $120^\circ$ , tip radius 200  $\mu\text{m}$ ). A progressive load up to 100 N, at a loading rate of 120 N/min and a horizontal displacement rate of 6 mm/min were applied. This resulted in a scratch length of 5 mm, which was evaluated in a light optical microscope to determine the critical load  $L_{C2}$  indicating where the adhesion failure occurred [52,53]. Each sample was scratched three times at each time point.

#### 2.6. Wear Resistance (2D) in a Hard-on-Soft Contact

Multidirectional wear tests (MWT) were carried out to evaluate the response of the coatings against polyethylene using cylindrical pins with a nominal length of 19.1 mm and diameter of 9.5 mm. The pins were made of UHMWPE GUR1020 (one of the two most commonly used grades of UHMWPE in orthopaedics, defined as per BS ISO 5834-2 2019 [54]), provided by the collaborating industrial partners Peter Brehm GmbH (Weisendorf, Germany). MWT tests were performed in 0.2  $\mu\text{m}$  filtered bovine serum solution (25%) at 37  $^\circ\text{C}$ . Prior to testing, the pins were presoaked in serum and cleaned according to standard [55]. The test was carried out with a nominal load of 150 N resulting in an estimated contact pressure of 2.1 MPa within the guidelines of [56], frequency 2 Hz, and sliding velocity 56 mm/s for 2,000,000 cycles (2.0 MC) using a 7 mm  $\times$  7 mm square path for a sliding distance of 28 mm/cycle.

#### 2.7. Statistical Analysis

IBM SPSS Statistics v 26 (New York, NY, USA) was used for all statistical analyses. An analysis of variance (ANOVA) was performed, followed by a Scheffe's post hoc test. When Levene's test for homogeneity of variances was significant, Welch's robust test followed by a Tamhane post hoc test was used instead. The Pearson correlation coefficient was used to evaluate potential correlations. A critical level of  $\alpha = 0.05$  was used to determine significance.

### 3. Results and Discussion

#### 3.1. Coating Thickness and Composition

The growth rate for the  $\text{SiN}_x$  coatings depended on applied target power settings and bias voltages, as well as the  $\text{N}_2$  and  $\text{C}_2\text{H}_2$  gas flows. Increased  $\text{SiN}_x$  and  $\text{SiMeN}_x$  growth rates resulted from more material being removed from the target due to elevated target potentials [57]. Additionally, as Nb or Cr were added to the process, the number of operated targets increased and contributed to the  $\text{SiMeN}_x$  growth. The growth rate for the different bias settings showed a maximum at a medium level, indicating that the flux of film-forming species at low bias voltages was not optimally directed to the substrate table and resputtering occurred at high bias voltage settings. Increasing amounts of  $\text{N}_2$  led to decreased growth rates due to target poisoning [47] while an increased  $\text{C}_2\text{H}_2$  gas flow resulted in an increased growth rate. This was attributed to a reduction in coating mass density and morphological density, specifically a pronounced growth of columns [45].

Following the trend of the coating growth rate, the coating composition changed by increasing  $\text{N}_2$  and  $\text{C}_2\text{H}_2$  gas flows, leading to increased amounts of N and C in the coating. XPS results showed a nitrogen content close to 50 at % for all coatings (Table 2).  $\text{SiN}_x$  coatings with a higher ion energy

and 40% of N<sub>2</sub> during deposition yielded a nitrogen content in the coatings exceeding 51 at % and a N/Si ratio  $\geq 1$ . This ratio has previously been shown to be beneficial to a lower dissolution rate, which could be advantageous to the coating lifespan [39]. When C<sub>2</sub>H<sub>2</sub> was added to the process the coating showed higher O contents, which in turn supported the interpretation for the growth rate of SiCN<sub>x</sub> at elevated C<sub>2</sub>H<sub>2</sub> flows. Here, the reduction in coating density and the pronounced growth of columns led to incorporation of O as the coatings were exposed to air prior to analysis. Further, a reduced morphological density was observed as Cr and Nb were added to the process [40]. This was mirrored in higher O and C contents in the corresponding coatings.

**Table 2.** Deposition settings, coating thicknesses, growth rates, and composition.

Coating Designation	Si Power (kW)	Bias	Settings		Elemental Composition—XPS					
			SiN/SiMeN/SiCN Thickness (μm)	Growth Rate (nm/s)	Si (at %)	N (at %)	O (at %)	C (at %)	Nb/Cr (at %)	N/Si -
Standard	5.0	low	5.5	0.13	42.8	49.7	5.5	2.0	-	1.16
N2-low	5.0	low	3.8	0.21	51.8	47.9	-	0.3	-	0.92
N2-medium	5.0	low	3.5	0.19	43.1	46.3	7.4	3.2	-	1.07
N2-high/Bias low/Standard	5.0	low	2.1	0.12	44.7	54.7	0.2	0.4	-	1.22
Bias-medium	5.0	medium	6.4	0.15	45.6	54.4	-	-	-	1.19
Bias-high	5.0	high	6.2	0.14	44.5	55.5	-	-	-	1.25
C-low, 2.5%	5	medium	5.4	0.17	33.1	47.2	2.9	16.9	-	1.43
C-high, 4%	5	medium	6.4	0.2	27.9	42.6	3.9	25.7	-	1.53
Nb-low, 2 × 1 kW Nb	5.0	low	3.1	0.17	39.9	46.8	3.6	1	7	1.17
Nb-medium, 2 × 2 kW Nb	5.0	low	3.1	0.17	33.9	45.2	4.2	1.3	13.7	1.33
Nb-high, 2 × 5 kW Nb	5.0	low	5.8	0.32	25.1	43.1	4.1	1.5	24.5	1.72
Cr-medium, 2 × 1 kW Cr	5.0	low	3.2	0.18	33.8	44.6	4.4	3.6	12.8	1.32
Si Power-high	8.0	low	4	0.24	46.5	52.3	1.2	-	-	1.12

The microstructure of similar coatings has been published earlier, for a range of coating parameters [47]. The SiN<sub>x</sub> coatings that performed well were very dense and, thus, had low O and C contents, but also displayed more residual stresses. Likewise the coatings that did not perform well were less dense and contained more O and C (by adsorption) [48].

### 3.2. Surface Roughness

The average surface roughness ( $R_a$ ) determined for the as-deposited coatings was <50 nm (Table 3), thus fulfilling the standard for biomedical implants (ASTM F2033-12). Coatings *C-low*, *Standard*, *Nb-medium*, and *Nb-high* displayed the lowest values (7.69–12.97 nm), followed by coatings *Nb-low*, *Si Power-high*, *Bias-medium*, *C-high*, and *i* (14.71–19.97 nm). The highest values of  $R_a$  were obtained for coatings *Bias-high*, *N-medium*, *N-low*, and *N-high* (22.2–42.05 nm). As shown in Table 3, the coatings with higher Nb and C content presented relatively low surface roughness values. A lower surface roughness could possibly be attributed to the ionization energy of N being higher than C, which resulted in more carbon atoms being deposited. On the other hand more of the amorphous phase was being created, resulting in a smoother surface [58–62]. No statistically significant correlation could be found between surface roughness and coating thickness, nor between surface roughness and deposition rate.

**Table 3.** Average surface roughness of SiN<sub>x</sub> coatings, as measured by interferometry. Coatings attributed with the same letters from a–e were not statistically significantly different (i.e.,  $p > 0.05$ ).

Coating Designation	R <sub>a</sub> (nm)	Statistical Differences
Uncoated CoCr	3.5 ± 0.2	<i>a</i>
Standard	10 ± 0.9	<i>b, c</i>
N-low	33.2 ± 2.9	-
N-medium	33.1 ± 12.4	<i>e</i>
N-high	42.0 ± 6.0	-
C-low	7.6 ± 0.5	<i>a, b</i>
C-high	18.8 ± 3.0	<i>d, e</i>
Nb-low	14.7 ± 0.7	<i>c, d</i>
Nb-medium	12.9 ± 0.4	<i>c</i>
Nb-high	10.1 ± 3.4	<i>b, c</i>
Cr	19.9 ± 0.8	<i>e</i>
Bias-medium	18.0 ± 1.1	<i>d, e</i>
Bias-high	22.2 ± 1.1	-
Si Power-high	16.8 ± 0.5	-

### 3.3. Mechanical Properties (Nanoindentation)

The coating hardness varied from 13–25.4 GPa, with coatings *Standard*, *N-high*, and *N-low* exhibiting higher values (Figure 1). A similar tendency could be observed for the Young's modulus.

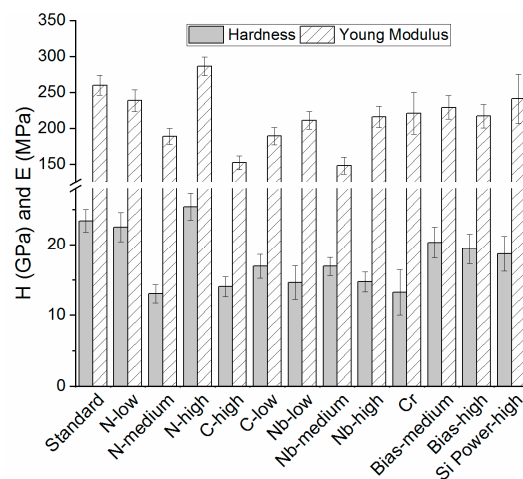


**Figure 1.** Hardness and Young's modulus for SiN<sub>x</sub> based coatings.

Earlier studies on SiN<sub>x</sub> coatings have determined similar values for hardness and Young's modulus, although different deposition methods were applied [39,44,47,63,64]. A higher hardness suggests a higher coating density. Hardness values reported for other coatings for joint implants such as ZrN, TiNbN, Ox-Zr, and TiN coatings resided in a similar range, namely 14.0–31.0, 14.0–24.5 and 12.0–14.0 and 33–56 GPa, respectively [65].

### 3.4. Adhesion

The scratch test results in terms of L<sub>c2</sub> values are shown in Figure 2. As can be seen, coatings deposited with a higher target power showed lower L<sub>c2</sub> values. This was due to higher residual stresses resulting from a higher N content and the increase in Si-N bonds [45,48]. Moreover, these coatings showed a generally denser morphology (data not shown), which in turn contributed to increased residual stresses [66], as demonstrated previously [48]. Furthermore, coatings with higher O and Cr contents displayed higher L<sub>c2</sub> values, which may be related to a lower amount of N-bonds, i.e., an opposite trend to that previously mentioned and/or a decreased coating density and, hence,

residual stresses. The following coatings showed statistical differences: *Standard* vs. *C-high*, *Nb-medium*, *Nb-high*, *Bias-medium*, *Bias-high*, and *Si power high* as well as *C-high* vs. *Nb-medium*, *Nb-high*, *Bias-high*, and *Si power high*.

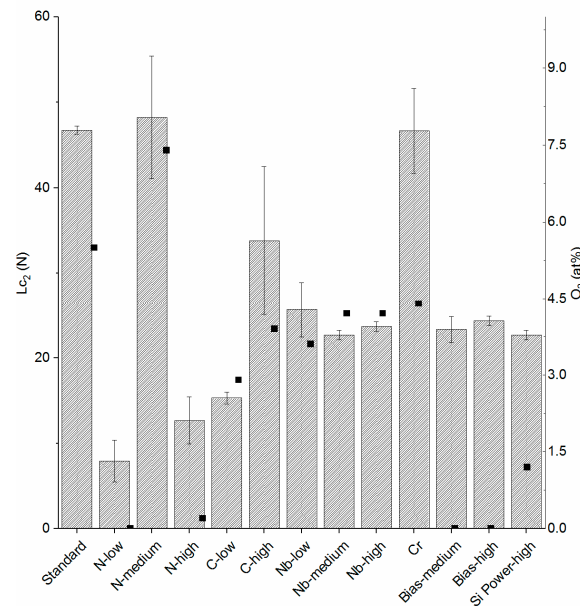


**Figure 2.** On the left axis the results for adhesion ( $L_{c2}$ ) are shown for the coatings tested in this study, with bars and standard deviations. On the right axis the  $O_2$  content of the coatings is shown, represented by square dots.

### 3.5. Multidirectional Wear Tests

#### 3.5.1. Macroscopic Appearance and Surface Analysis

The macroscopic surface structure of the coatings after the wear tests is shown in Figure 3. The formation of an opaque layer on the surface could be observed during testing on some of the coatings (Figure 3). XPS measurements were, therefore, performed on coating *N-medium*, at a region that still displayed a reflective surface (assumed to be unworn) and a region that had formed an opaque layer on the surface. Previous work showed a tribofilm formation in aqueous environments for  $Si_3N_4$  materials, and in those conditions a  $SiO_2$  and  $Si(OH)_2$  layer could be found, improving the wear resistance and reducing the coefficient of friction by acting as a self-lubricating layer [67–69]. However, in the XPS measurements herein the use of charge neutralizers and lack of a good charge reference made the positions of the peaks uncertain. To determine whether the  $Si2p$  and  $O1s$  peaks originated from Si-O bonds, the distance between the peaks,  $\Delta E_b$ , was determined and compared to the distance ( $\Delta E_b$ ) from literature according to Briggs et al. [70]. The deconvoluted Si peaks were fitted with the smallest number of curves possible. The spectrum obtained at the surface revealed contributions attributed to Si-C (100.8 eV), Si-N (101.4 eV), and Si-O (102.8 eV), which correlated well with findings from similar materials. After 2 min sputtering at 500 V the Si-O contribution was no longer detected, while there were still contributions attributed to Si-N and Si-C, and after additional sputtering for 20 min at 1 kV only two contributions were identified, Si-N and Si-Si. These results indicated that the outer layer contained more O and C compared to the bulk of the coating, which could be due to the formation of a tribofilm during wear testing.

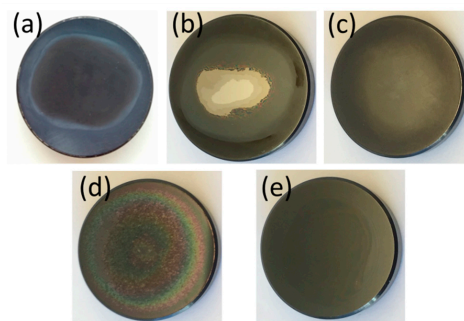


**Figure 3.** Typical macroscopic appearances of (a) a reacted surface (Standard), (b) a failed coating (Nb-medium), and (c,d) coatings with a surface layer: (c) Coating Cr and (d) coating Si Power-high. In (e) a Bias-high coating is shown, which did not present any layer formation or upcoming failure up to 2 MC.

### 3.5.2. Coefficient of Friction

Low coefficients of friction were observed for the first 0.5 million cycles for *N-high*, *Standard*, *Bias-medium*, and *Bias-high* (0.051–0.067). Coatings *N-low*, *Cr*, and *Si Power-high* showed somewhat higher values, from 0.103–0.108, with little variation. Coefficients of friction did not change markedly throughout the tests, except for coatings that reacted or failed during the test (Figure 4). This work generally showed lower coefficients of friction compared to previous work on Nb-Ti-N coatings (ranging from 0.11 to 0.12) and on TiN (0.14) [66].

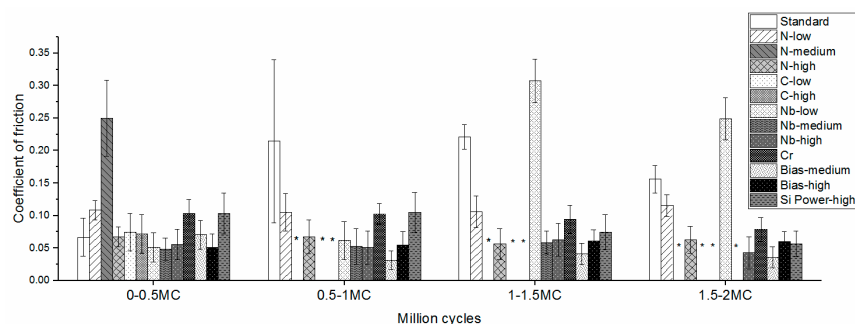


**Figure 4.** Coefficient of friction up to 2.0 MC for the tested coatings. During wear tests the following coatings wore through: (\*) *N-medium*, *C-high*, and *C-low* at 0.5 MC; *Nb-medium* at 1.5 MC; *Nb-low* and *Nb-high* at 2.0 MC.

### 3.5.3. Volumetric Wear Rate

While *N-low* and *N-high* gave the lowest wear rates for the UHMWPE pins ( $< 0.37 \text{ mm}^3/\text{MC}$ , Figure 4), *N-medium* failed already in the first 0.5 MC (Figure 3), giving a high wear rate due to the increased surface roughness from the reacted surface. The *Standard* coating also gave a high wear rate, due to a reacted surface (Figure 3). The coatings with a higher C content all failed at 0.5 MC. Nb coatings failed at different time points, for example, *Nb-low* and *Nb-high* had failed at 2.0 MC and *Nb-medium* at 1.5 MC. The remaining coatings did not fail and presented low wear rates ( $0.74\text{--}3.63 \text{ mm}^3/\text{MC}$ ). Figures 3 and 5 show that coatings with no apparent reaction or coating failure, and that gave low pin wear rates, were those with an initially high hardness (22.5–28.4 GPa), and, hence, presumably higher density and lower reactivity and/or a high N content (*N-low*, *N-high*, *Bias-medium*, *Bias-high*, and *Si Power-high*), with the exception being the *Standard* ( $H = 23.4 \text{ GPa}$ ) coating, which, however, contained more oxygen than the well-performing coatings (Table 2), suggesting a higher reactivity. Coating wear through contact with UHMWPE during the tests was not expected, and coatings failing would rather be associated to a higher reactivity and subsequent dissolution [40].



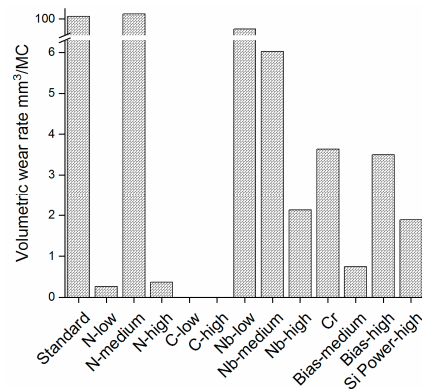


**Figure 5.** Volumetric wear rate for the UHMWPE pins ran against all coatings in this study. Coatings C-high and C-low showed negative values of  $-2.90$  and  $-8.40$   $\text{mm}^3/\text{MC}$ , respectively.

#### 4. Conclusions

Based on the results of the coatings tested in this work, some important conclusions were drawn. First, the low-ion energy coatings generally exhibited a lower hardness and initially higher critical load in scratch testing. High concentrations of impurities (higher O content and lower N content) were associated with early reactions and/or dissolution of the coating, as shown by XPS compositional analysis as well as multidirectional wear tests. During the wear tests coatings with lower or no apparent O content did not fail and showed a low volumetric wear rate of UHMWPE pins.  $\text{SiN}_x$  coatings of high N content, low O content (e.g., *N-high*, *Bias-medium*, *Bias-high*, and *Si Power-high*) are needed for the target-joint implant applications. Promising low wear rates were found for UHMWPE pins sliding against these latter coatings in a multidirectional wear test.

#### 5. Patents

Ionbond AG, where S.S. and M.T. are employees, owns patents related to similar coatings.

**Author Contributions:** Conceptualization, C.G., M.T., S.S., H.E., H.H., and C.P.; methodology, L.C.F., C.S., M.T., S.S., and C.P.; validation, L.C.F., C.G., C.S., M.T., and S.S.; formal analysis, L.C.F., C.G., C.S., M.T., S.S., and C.P.; investigation, L.C.F., C.G., C.S., M.T., and S.S.; resources, C.P., H.H., and H.E.; writing—original draft preparation, L.C.F., M.T., S.S., and C.P.; writing—review and editing, L.C.F., S.S., C.G., C.S., H.E., M.T., H.H., and C.P.; visualization, L.C.F., S.S., and C.P.; supervision, H.E., H.H., and C.P.; project administration, H.H., H.E., and C.P.; funding acquisition, C.P., H.E., and H.H. All authors have read and agreed to the published version of the manuscript.

**Funding:** This research was funded by the European Union, grant number FP7-NMP-2012-310477 (Life Long Joints project); EBW+ Project Erasmus Mundus Programme, Action 2–STRAND 1, Lot 9 (Latin America), Brazil, Grant number 2014-0982. H.H. acknowledges financial support from the Swedish Government Strategic Research Area in Materials Science on Advanced Functional Materials at Linköping University (Faculty Grant SFO Mat LiU No. 2009 00971).

**Acknowledgments:** The authors are grateful for assistance from Mathilde Cogrel and Alejandro López for assistance with MWT measurements.

**Conflicts of Interest:** The authors declare no conflict of interest, and Ionbond AG, where S.S. and M.T. are employees, owns patents related to similar coatings.

#### References

- De Bellis, U.G.; Legnani, C.; Calori, G.M. Acute total hip replacement for acetabular fractures: A systematic review of the literature. *Injury* **2014**, *45*, 356–361. [[CrossRef](#)] [[PubMed](#)]
- Katz, J.N. Total joint replacement in osteoarthritis. *Best Pract. Res. Clin. Rheumatol.* **2006**, *20*, 145–153. [[CrossRef](#)] [[PubMed](#)]
- Salih, S.; Hamer, A. Hip and knee replacement. *Surgery* **2013**, *31*, 482–487. [[CrossRef](#)]
- Shan, L.; Shan, B.; Graham, D.; Saxena, A. Total hip replacement: A systematic review and meta-analysis on mid-term quality of life. *Osteoarthr. Cartil.* **2014**, *i22*, 389–406. [[CrossRef](#)] [[PubMed](#)]

5. Martinez-Cano, J.P.; Herrera-Escobar, J.P.; Arango Gutierrez, A.S.; Sanchez Vergel, A.; Martinez-Rondanelli, A. Prospective quality of life assessment after hip and knee arthroplasty: short- and mid-term follow-up results. *Arthroplast. Today* **2017**. [[CrossRef](#)] [[PubMed](#)]
6. Kärrholm, J.; Mohaddes, M.; Odén, D.; Vinblad, J.; Rogmark, C.; Rolfson, O. *Swedish Hip Arthroplasty Register Annual Report 2017*; Swedish Hip Arthroplasty Register: Göteborg, Sweden, 2017; ISBN 9789188017208.
7. Robertsson, O.; W-Dahl, A.; Lidgren, L.; Sundberg, M. *Swedish Knee Arthroplasty Register Annual Report 2018*; Swedish Hip Arthroplasty Register: Göteborg, Sweden, 2018.
8. Sharma, V.; Chang, J.-D.; Kim, I.-S.; Yoo, J.-H.; Lee, S.-S.; Mansukhani, S.A. Midterm outcome of fourth-generation ceramic-on-ceramic bearing surfaces in revision total hip arthroplasty. *J. Orthop. Surg.* **2018**, *26*, 230949901878391. [[CrossRef](#)]
9. Kurtz, S.M.; Kocagöz, S.; Arnholt, C.; Huet, R.; Ueno, M.; Walter, W.L. Advances in zirconia toughened alumina biomaterials for total joint replacement. *J. Mech. Behav. Biomed. Mater.* **2014**. [[CrossRef](#)]
10. Gamble, D.; Jaiswal, P.K.; Lutz, I.; Johnston, K.D. The Use of Ceramics in Total Hip Arthroplasty. *Orthop. Rheumatol.* **2017**, *4*, 1–7. [[CrossRef](#)]
11. Maheshwari, A.V.; Shah, N.V.; Newman, J.M.; Pascal, S.; Sheth, N.P.; Grieco, P.W.; Stroud, S.G. New alternate bearing surfaces in total hip arthroplasty: A review of the current literature. *J. Clin. Orthop. Trauma* **2017**, *9*, 7–16. [[CrossRef](#)]
12. Kumar, N.; Arora, N.C.; Datta, B. Bearing surfaces in hip replacement—Evolution and likely future. *Med. J. Armed Forces India* **2014**, *70*, 371–376. [[CrossRef](#)]
13. Garrett, S.; Jacobs, N.; Yates, P.; Smith, A.; Wood, D. Differences in metal ion release following cobalt-chromium and oxidized zirconium total knee arthroplasty. *Acta Orthop. Belg.* **2010**, *76*, 513–520. [[PubMed](#)]
14. Hui, C.; Salmon, L.; Maeno, S.; Roe, J.; Walsh, W.; Pinczewski, L. Five-Year Comparison of Oxidized Zirconium and Cobalt-Chromium Femoral Components in Total Knee Arthroplasty: A Randomized Controlled Trial. *JBJS* **2011**, *93*, 624–630. [[CrossRef](#)] [[PubMed](#)]
15. Nowakowski, A.M.; Vavken, P.; Pagenstert, G.; Valderrabano, V. Design, Shape, and Materials of Total Knee Replacement. In *The Unhappy Total Knee Replacement: A Comprehensive Review and Management Guide*; Hirschmann, M.T., Becker, R., Eds.; Springer International Publishing: Cham, Switzerland, 2015; ISBN 978-3-319-08099-4.
16. Meier, E.; Gelse, K.; Trieb, K.; Pachowsky, M.; Hennig, F.F.; Mauerer, A. First clinical study of a novel complete metal-free ceramic total knee replacement system. *J. Orthop. Surg. Res.* **2016**, *11*, 21. [[CrossRef](#)]
17. Haider, H.; Weisenburger, J.N.; Namavar, F.; Garvin, K.L. Why Coating Technologies for Hip Replacement Systems, and the Importance of Testing Them In Vitro. *Oper. Tech. Orthop.* **2017**, *27*, 152–160. [[CrossRef](#)]
18. Wang, Y.X.; Zhang, S. Toward hard yet tough ceramic coatings. *Surf. Coat. Technol.* **2014**, *258*, 1–16. [[CrossRef](#)]
19. Breugem, S.J.M.; Linnartz, J.; Siervelt, I.; Bruijn, J.D.; Driessen, M.J.M. Evaluation of 1031 primary titanium nitride coated mobile bearing total knee arthroplasties in an orthopedic clinic. *World J. Orthop.* **2017**, *8*, 922–928. [[CrossRef](#)]
20. Mohammed, A.; Metcalfe, A.; Woodnutt, D. Medium-term outcome of titanium nitride, mobile bearing total knee replacement. *Acta Orthop. Belg.* **2014**, *80*, 269–275.
21. Fabry, C.; Zietz, C.; Baumann, A.; Ehall, R.; Bader, R. High wear resistance of femoral components coated with titanium nitride: a retrieval analysis. *Knee Surg. Sport. Traumatol. Arthrosc.* **2018**, *26*, 2630–2639. [[CrossRef](#)]
22. Thomsen, M.; Rozak, M.; Thomas, P. Pain in a chromium-allergic patient with total knee arthroplasty: disappearance of symptoms after revision with a special surface-coated TKA—A case report. *Acta Orthop.* **2011**, *82*, 386–388. [[CrossRef](#)]
23. Lützner, J.; Dinnebier, G.; Hartmann, A.; Günther, K.-P.; Kirschner, S. Study rationale and protocol: prospective randomized comparison of metal ion concentrations in the patient's plasma after implantation of coated and uncoated total knee prostheses. *BMC Musculoskelet. Disord.* **2009**, *10*, 128. [[CrossRef](#)]
24. Spector, M.; Ries, M.D.; Bourne, R.B.; Sauer, W.S.; Long, M.; Hunter, G. Wear performance of ultra-high molecular weight polyethylene, on oxidized zirconium total knee femoral components. *JBJS* **2001**, *83*, S80–S86. [[CrossRef](#)] [[PubMed](#)]
25. Hauert, R.; Thorwarth, K.; Thorwarth, G. An overview on diamond-like carbon coatings in medical applications. *Surf. Coat. Technol.* **2013**. [[CrossRef](#)]
26. Hendry, J.A.; Pilliar, R.M. The fretting corrosion resistance of PVD surface-modified orthopedic implant alloys. *J. Biomed. Mater. Res.* **2001**, *58*, 156–166. [[CrossRef](#)]

27. Bader, R.; Bergschmidt, P.; Fritsche, A.; Ansorge, S.; Thomas, P.; Mittelmeier, W. Alternative Werkstoffe und Lösungen in der Knieendoprothetik für Patienten mit Metallallergie. *Orthopade* **2008**, *37*, 136–142. [[CrossRef](#)] [[PubMed](#)]
28. Alakoski, E.; Tiainen, V.-M.; Soininen, A.; Konttinen, Y.T. Load-Bearing Biomedical Applications of Diamond-Like Carbon Coatings - Current Status. *Open Orthop. J.* **2008**. [[CrossRef](#)]
29. Dearnaley, G.; Arps, J.H. Biomedical applications of diamond-like carbon (DLC) coatings: A review. *Surf. Coat. Technol.* **2005**. [[CrossRef](#)]
30. Maru, M.M.; Amaral, M.; Rodrigues, S.P.; Santos, R.; Gouvea, C.P.; Archanjo, B.S.; Trommer, R.M.; Oliveira, F.J.; Silva, R.F.; Achete, C.A. The High performance of nanocrystalline CVD diamond coated hip joints in wear simulator test. *J. Mech. Behav. Biomed. Mater.* **2015**. [[CrossRef](#)]
31. Pappas, M.J.; Makris, G.; Buechel, F.F. Titanium nitride ceramic film against polyethylene. A 48 million cycle wear test. *Clin. Orthop. Relat. Res.* **1995**, *317*, 64–70.
32. Ching, H.A.; Choudhury, D.; Nine, M.J.; Abu Osman, N.A. Effects of surface coating on reducing friction and wear of orthopaedic implants. *Sci. Technol. Adv. Mater.* **2014**, *15*. [[CrossRef](#)]
33. Leslie, I.; Williams, S.; Isaac, G.; Hatto, P.; Ingham, E.; Fisher, J. Wear of surface-engineered metal-on-metal bearings for hip prostheses under adverse conditions with the head loading on the rim of the cup. *Proc. Inst. Mech. Eng. Part H J. Eng. Med.* **2013**. [[CrossRef](#)]
34. Van Hove, R.P.; Sierevelt, I.N.; van Royen, B.J.; Nolte, P.A. Titanium-nitride coating of orthopaedic implants: a review of the literature. *Biomed. Res. Int.* **2015**, *2015*, 9. [[CrossRef](#)] [[PubMed](#)]
35. Nelissen, R.G.H.H.; Valstar, E.R.; Rozing, P.M. The effect of hydroxyapatite on the micromotion of total knee prostheses. A prospective, randomized, double-blind study. *JBS* **1998**, *80*, 1665–1672. [[CrossRef](#)] [[PubMed](#)]
36. Bal, B.S.; Rahaman, M.N. Orthopedic applications of silicon nitride ceramics. *Acta Biomater.* **2012**, *8*, 2889–2898. [[CrossRef](#)] [[PubMed](#)]
37. Bock, R.M.; McEntire, B.J.; Bal, B.S.; Rahaman, M.N.; Boffelli, M.; Pezzotti, G. Surface modulation of silicon nitride ceramics for orthopaedic applications. *Acta Biomater.* **2015**. [[CrossRef](#)]
38. Pettersson, M.; Bryant, M.; Schmidt, S.; Engqvist, H.; Hall, R.M.; Neville, A.; Persson, C. Dissolution behaviour of silicon nitride coatings for joint replacements. *Mater. Sci. Eng. C* **2016**, *62*, 497–505. [[CrossRef](#)]
39. Pettersson, M.; Tkachenko, S.; Schmidt, S.; Berling, T.; Jacobson, S.; Hultman, L.; Engqvist, H.; Persson, C. Mechanical and tribological behavior of silicon nitride and silicon carbon nitride coatings for total joint replacements. *J. Mech. Behav. Biomed. Mater.* **2013**, *25*, 41–47. [[CrossRef](#)]
40. Filho, L.C.; Schmidt, S.; López, A.; Cogrel, M.; Leifer, K.; Engqvist, H.; Högberg, H.; Persson, C. The Effect of Coating Density on Functional Properties of SiN(x) Coated Implants. *Materials* **2019**, *12*, 3370. [[CrossRef](#)]
41. Lee, J.-W.; Chang, Y.-C. A study on the microstructures and mechanical properties of pulsed DC reactive magnetron sputtered Cr-Si-N nanocomposite coatings. *Surf. Coat. Technol.* **2007**, *202*, 831–836. [[CrossRef](#)]
42. Park, J.H.; Chung, W.S.; Cho, Y.-R.; Kim, K.H. Synthesis and mechanical properties of Cr-Si-N coatings deposited by a hybrid system of arc ion plating and sputtering techniques. *Surf. Coat. Technol.* **2004**, *188*, 425–430. [[CrossRef](#)]
43. Hones, P.; Sanjines, R.; Lévy, F. Sputter deposited chromium nitride based ternary compounds for hard coatings. *Thin Solid Films* **1998**, *332*, 240–246. [[CrossRef](#)]
44. Olofsson, J.; Pettersson, M.; Teuscher, N.; Heilmann, A.; Larsson, K.; Grandfield, K.; Persson, C.; Jacobson, S.; Engqvist, H. Fabrication and evaluation of SixNy coatings for total joint replacements. *J. Mater. Sci. Mater. Med.* **2012**, *23*, 1879–1889. [[CrossRef](#)] [[PubMed](#)]
45. Hänninen, T.; Schmidt, S.; Ivanov, I.G.; Jensen, J.; Hultman, L.; Högberg, H. Silicon carbonitride thin films deposited by reactive high power impulse magnetron sputtering. *Surf. Coat. Technol.* **2018**, *335*, 248–256. [[CrossRef](#)]
46. Skjöldebrand, C.; Schmidt, S.; Vuong, V.; Pettersson, M.; Grandfield, K.; Högberg, H.; Engqvist, H.; Persson, C. Influence of substrate heating and nitrogen flow on the composition, morphological and mechanical properties of SiNx coatings aimed for joint replacements. *Materials* **2017**, *10*, 173. [[CrossRef](#)] [[PubMed](#)]
47. Schmidt, S.; Hänninen, T.; Goyenola, C.; Wissting, J.; Jensen, J.; Hultman, L.; Goebbels, N.; Tobler, M.; Högberg, H. SiN x Coatings Deposited by Reactive High Power Impulse Magnetron Sputtering: Process Parameters Influencing the Nitrogen Content. *ACS Appl. Mater. Interfaces* **2016**. [[CrossRef](#)] [[PubMed](#)]

48. Schmidt, S.; Hänninen, T.; Wissting, J.; Hultman, L.; Goebbels, N.; Santana, A.; Tobler, M.; Högberg, H. SiN<sub>x</sub> coatings deposited by reactive high power impulse magnetron sputtering: Process parameters influencing the residual coating stress. *J. Appl. Phys.* **2017**, *121*, 171904. [[CrossRef](#)]
49. Hofmann, S. *Auger- and X-ray Photoelectron Spectroscopy in Materials Science: A User-Oriented Guide*; Springer Science & Business Media: Berlin/Heidelberg, Germany, 2012; Volume 49.
50. Oliver, W. Improved technique for determining hardness and elastic modulus using load and displacement sensing indentation experiments. *J. Mater. Res.* **1992**. [[CrossRef](#)]
51. ISO 20502:2005. *Fine Ceramics (Advanced Ceramics, Advanced Technical Ceramics)—Determination of Adhesion of Ceramic Coatings by Scratch Testing*; ISO: Geneva, Switzerland, 2005.
52. Hassan, M.A.; Bushroa, A.R.; Mahmoodian, R. Identification of critical load for scratch adhesion strength of nitride-based thin films using wavelet analysis and a proposed analytical model. *Surf. Coat. Technol.* **2015**, *277*, 216–221. [[CrossRef](#)]
53. Beake, B.D.; Vishnyakov, V.M.; Valizadeh, R.; Colligon, J.S. Influence of mechanical properties on the nanoscratch behaviour of hard nanocomposite TiN/Si<sub>3</sub>N<sub>4</sub> coatings on Si. *J. Phys. D: Appl. Phys.* **2006**, *39*, 1392. [[CrossRef](#)]
54. ISO 5834-2:2019. *Implants for Surgery—Ultra-High-Molecular-Weight Polyethylene—Part 2: Moulded Forms*; ISO: Geneva, Switzerland, 2019.
55. ASTM. *ASTM F2025-06(2018), Standard Practice for Gravimetric Measurement of Polymeric Components for Wear Assessment*; ASTM International: West Conshohocken, PA, USA, 2018. [[CrossRef](#)]
56. ASTM. *ASTM F732-17, Standard Test Method for Wear Testing of Polymeric Materials Used in Total Joint Prostheses*; ASTM International: West Conshohocken, PA, USA, 2017.
57. Wasa, K.; Hayakawa, S. *Handbook of Sputter Deposition Technology*; IAEA: Vienna, Austria, 1992.
58. Gu, J.; Li, L.; Miao, H.; Xu, Y.; Xu, Y.; Sun, J.; Wang, X.; He, Z. Effect of C<sub>2</sub>H<sub>2</sub>/N<sub>2</sub> partial pressure ratio on microstructure and mechanical properties of Ti-Al-Si-C-N coatings. *Surf. Coat. Technol.* **2019**, *365*, 200–207. [[CrossRef](#)]
59. Huang, S.W.; Ng, M.W.; Samandi, M.; Brandt, M. Tribological behaviour and microstructure of TiC<sub>x</sub>N(1-x) coatings deposited by filtered arc. *Wear* **2002**, *252*, 566–579. [[CrossRef](#)]
60. Guo, C.; Li, M.; Nibarger, J.P.; Gibson, G.N. Single and double ionization of diatomic molecules in strong laser fields. *Phys. Rev. A* **1998**, *58*, R4271–R4274. [[CrossRef](#)]
61. Sorensen, S.L.; Björneholm, O.; Hjelte, I.; Kihlgren, T.; Öhrwall, G.; Sundin, S.; Svensson, S.; Buil, S.; Descamps, D.; L’Huillier, A.; et al. Femtosecond pump-probe photoelectron spectroscopy of predissociative Rydberg states in acetylene. *J. Chem. Phys.* **2000**, *112*, 8038–8042. [[CrossRef](#)]
62. Reutt, J.E.; Wang, L.S.; Pollard, J.E.; Trevor, D.J.; Lee, Y.T.; Shirley, D.A. Photoelectron spectroscopy and inferred femtosecond intramolecular dynamics of C<sub>2</sub>H<sub>2</sub><sup>+</sup> and C<sub>2</sub>D<sub>2</sub><sup>+</sup>. *J. Chem. Phys.* **1986**, *84*, 3022–3031. [[CrossRef](#)]
63. Pusch, C.; Hoche, H.; Berger, C.; Riedel, R.; Ionescu, E.; Klein, A. Influence of the PVD sputtering method on structural characteristics of SiCN-coatings—Comparison of RF, DC and HiPIMS sputtering and target configurations. *Surf. Coat. Technol.* **2011**, *205*, S119–S123.
64. Shi, Z.; Wang, Y.; Du, C.; Huang, N.; Wang, L.; Ning, C. Silicon nitride films for the protective functional coating: blood compatibility and biomechanical property study. *J. Mech. Behav. Biomed. Mater.* **2012**, *16*, 9–20. [[PubMed](#)]
65. McEntire, B.J.; Bal, B.S.; Rahaman, M.N.; Chevalier, J.; Pezzotti, G. Ceramics and ceramic coatings in orthopaedics. *J. Eur. Ceram. Soc.* **2015**, *35*, 4327–4369.
66. Dumitriu La Grange, D.; Goebbels, N.; Santana, A.; Heuberger, R.; Imwinkelried, T.; Eschbach, L.; Karimi, A. Effect of niobium onto the tribological behavior of cathodic arc deposited Nb-Ti-N coatings. *Wear* **2016**, *368–369*. [[CrossRef](#)]
67. Park, I.-W.; Kang, D.S.; Moore, J.J.; Kwon, S.C.; Rha, J.J.; Kim, K.H. Microstructures, mechanical properties, and tribological behaviors of Cr-Al-N, Cr-Si-N, and Cr-Al-Si-N coatings by a hybrid coating system. *Surf. Coat. Technol.* **2007**, *201*, 5223–5227. [[CrossRef](#)]
68. Xu, J.; Kato, K. Formation of tribochemical layer of ceramics sliding in water and its role for low friction. *Wear* **2000**, *245*, 61–75. [[CrossRef](#)]

69. Dante, R.C.; Kajdas, C.K. A review and a fundamental theory of silicon nitride tribochemistry. *Wear* **2012**. [[CrossRef](#)]
70. Briggs, D. *Handbook of X-ray Photoelectron Spectroscopy*; Wanger, C.D., Riggs, W.M., Davis, L.E., Moulder, J.F., Muilenberg, G.E., Eds.; Perkin-Elmer Corp., Physical Electronics Division: Eden Prairie, MN, USA, 1979; pp. 190–195.



© 2020 by the authors. Licensee MDPI, Basel, Switzerland. This article is an open access article distributed under the terms and conditions of the Creative Commons Attribution (CC BY) license (<http://creativecommons.org/licenses/by/4.0/>).